Synthesis of S-doped graphene by liquid precursor

2012 Nanotechnology 23 275605

(http://iopscience.iop.org/0957-4484/23/27/275605)

Nanotechnology **23** (2012) 275605 (7pp) doi:10.1088/0957-4484/23/27/275605

Synthesis of S-doped graphene by liquid precursor

Hui Gao[1,2,5], Zheng Liu[2,5], Li Song[2], Wenhua Guo[3], Wei Gao[2], Lijie Ci[2], Amrita Rao[4], Weijin Quan[2], Robert Vajtai[2] and Pulickel M Ajayan[2]

[1] Department of Materials Science, School of Physical Science and Technology, Lanzhou University, Lanzhou 730000, People's Republic of China
[2] Department of Mechanical Engineering and Materials Science, Rice University, Houston, TX 77005, USA
[3] Share Equipment Authority SEA, Rice University, Houston, TX 77005, USA
[4] The Lawrenceville School, Lawrenceville, NJ 08648, USA

E-mail: hope@lzu.edu.cn and ajayan@rice.edu

Received 22 February 2012, in final form 8 May 2012
Published 19 June 2012
Online at stacks.iop.org/Nano/23/275605

Abstract
Doping is a common and effective approach to tailor semiconductor properties. Here, we demonstrate the growth of large-area sulfur (S)-doped graphene sheets on copper substrate via the chemical vapor deposition technique by using liquid organics (hexane in the presence of S) as the precursor. We found that S could be doped into graphene's lattice and mainly formed linear nanodomains, which was proved by elemental analysis, high resolution transmission microscopy and Raman spectra. Measurements on S-doped graphene field-effect transistors (G-FETs) revealed that S-doped graphene exhibited lower conductivity and distinctive p-type semiconductor properties compared with those of pristine graphene. Our approach has produced a new member in the family of graphene based materials and is promising for producing graphene based devices for multiple applications.

(Some figures may appear in colour only in the online journal)

1. Introduction

Graphene, a honeycomb lattice formed by two-dimensional (2D) carbon, has attracted great interest for its prominent electronic properties including high mobility (1.5×10^4 cm^2 V^{-1} s^{-1}) and room-temperature quantum Hall effect [1]. Graphene is a zero-gap semiconductor, and the valence band intersects with the conduction band at K and K′ points in reciprocal space. Engineering the energy gap in graphene could improve the on/off ratio for the graphene field-effect transistor (G-FET), and therefore offer more potential applications in electronic devices [2]. Heteroatom doping is a promising approach for this goal. So far, different experimental strategies have been employed, mainly of substitution by nitrogen (N) or boron (B) doping in graphene. However, the case for sulfur (S) doping is quite different, compared with B and N. The S atom is much larger than the C atom, and the difference of electronegativity between C (2.55) and S (2.58) appears to be too small to offer significant charge transfer in C–S composites [3]. From an energetic standpoint, chemical doping of S into graphene's framework would seem to be quite difficult. However, the incorporation of S atoms in graphene is of crucial importance. Theoretical calculation has indicated that the structure of graphene would be distorted with S doping and thus open the band gap of graphene. This is essential for facilitating its applications in electronics [4, 5]. The investigation of S-doped graphene is also interesting and meaningful for modifying the local chemical reactivity of graphene, which would serve as a good sensor for polluting gases as well, like NO and NO_2 [6, 7].

To date, there have been several reports about S-doped carbon materials. For example, S-doped diamond films have been successfully synthesized through various chemical vapor deposition (CVD) techniques. These results revealed the potential of S to serve as a shallow-level donor in diamond [8, 9]. Doping of S would also induce significant changes in the

[5] These authors contributed equally to this work.

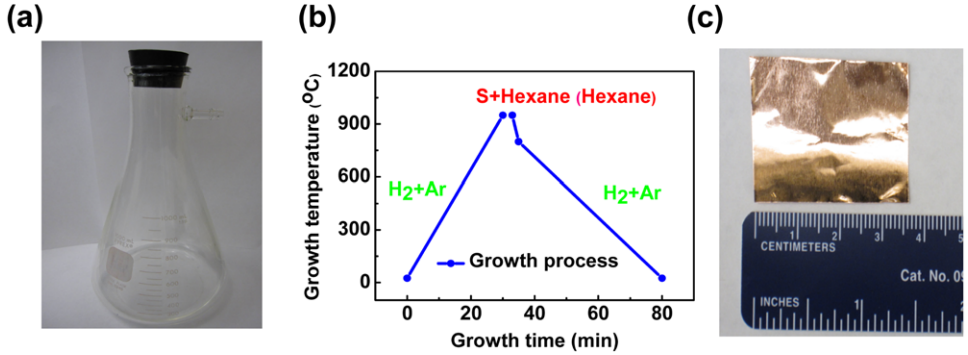

Figure 1. Synthesis process of S-doped graphene. (a) The mixture liquid precursor in the conical flask. (b) Digital photograph of graphene film grown on Cu substrate. (c) A schematic representation of the growth process of S-doped graphene or graphene.

electronic properties of fullerenes [10]. It has been reported that S-doped graphite exhibited superconducting behavior below 35 K [11, 12]. However, only small amounts of S or S-containing groups could be attached onto the C atoms due to the small binding energies between S and C nanotubes (CNTs) [13]. It is still a challenge to incorporate S into the CNTs' framework and graphene. In this paper, S-doped graphene sheets were synthesized by CVD technology by using a mixture of liquid organics and S as the growth precursor. Liquid precursor based growth can help in realizing S doping and graphene growth simultaneously. Moreover, in our investigation, besides the absorption of S, some S atoms, as a nanodomain, are also incorporated into graphene's lattice.

2. Experimental procedure

Sulfur powder was dissolved in the hexane under ultrasound for 15 min to form a transparent liquid, which was used as the growth precursor. Cu foil was placed in a quartz tube, and the whole system was pumped down to 10^{-2} Torr. The substrate was heated up with a flow of hydrogen and argon mixture (volume ratio 1:5) at a pressure of ∼10–11 Torr. When the temperature reached 950 °C, the H_2–Ar flow was shut off and S–hexane mixture vapor (the flow rate of hexane was about 4 ml h^{-1}) was introduced into the reaction chamber. After 2.5 min of growth, the sample was rapidly cooled down to 800 °C, and then the whole system was cooled down to room temperature with the hydrogen and argon atmosphere flowing (at a pressure of ∼10–11 Torr). The pristine graphene films were synthesized by the same route as the control sample. Both pristine graphene and S-doped graphene could be easily transferred onto SiO_2–Si substrate using PMMA as a supporting layer.

The samples were characterized by Raman spectroscopy (Renishaw inVia, with laser wavelength 514.5 nm), x-ray photoelectron spectroscopy (XPS, PHI Quantera), and scanning electron microscopy (SEM, FEI Quanta 400 ESEM FEG) with x-ray energy dispersive spectrometry (EDS) and high resolution transmission electron microscopy (HRTEM, JEM 2100F).

We also fabricated the S-doped graphene based bottom-gated field-effect transistor (FET) devices. The film with a size larger than 5 mm × 5 mm was firstly transferred onto SiO_2–Si. Patterned Ni–Au electrodes (5 nm–80 nm) were made on the film by the photolithography process and an e-beam evaporator. The evaporating rate was well controlled at about 1 Å s^{-1}. Then, the photoresist (S-1813) ribbon was patterned across the electrodes, and oxygen plasma cleaner was employed to etch away the film in the region with no photoresist-covering for 3 min. Finally, the rest of the photoresist could be removed by acetone, only leaving the graphene ribbon.

3. Results and discussion

The transparent liquid precursor (the mixture of S and hexane), a schematic representation of the growth process and the as-grown film on Cu foil for S-doped graphene are shown in figures 1(a)–(c), respectively. We choose Cu foil as the growth substrate because C has a lower solubility in Cu than in Ni, so we could obtain monolayer graphene much more easily.

The morphology and thickness of S-doped graphene sheets were evaluated by color contrast under an optical microscope. Figure 2(a) shows a uniform and continuous S-doped graphene sheet. The as-prepared sheet is predominantly monolayer, which was proved by Raman spectra and HRTEM analysis later. Sulfur is known to act as a cross-linker to promote the graphitization of C materials [12], and our results indicated that the existence of S could help the surface mediation and self-limiting of graphene growth. Figure 2(b) shows a typical SEM image of S-doped graphene. We observed that absorbed particles existed on the surface of graphene, and the particles were the aggregates of S. A typical EDS spectrum (figure 2(c)) shows the distinctive existence of S.

Raman spectroscopy is normally used to evaluate the thickness or doping information of graphene. Figure 3(a) compares the Raman spectra of pristine graphene and S-doped graphene. In the 1000–3000 cm^{-1} region, three typical features were observed for both samples, which corresponded to the D band (defects in sp^2 C), G band (doubly degenerate zone center E_{2g} mode, evidencing the formation of the C hexagonal lattice) and 2D band (the second order of

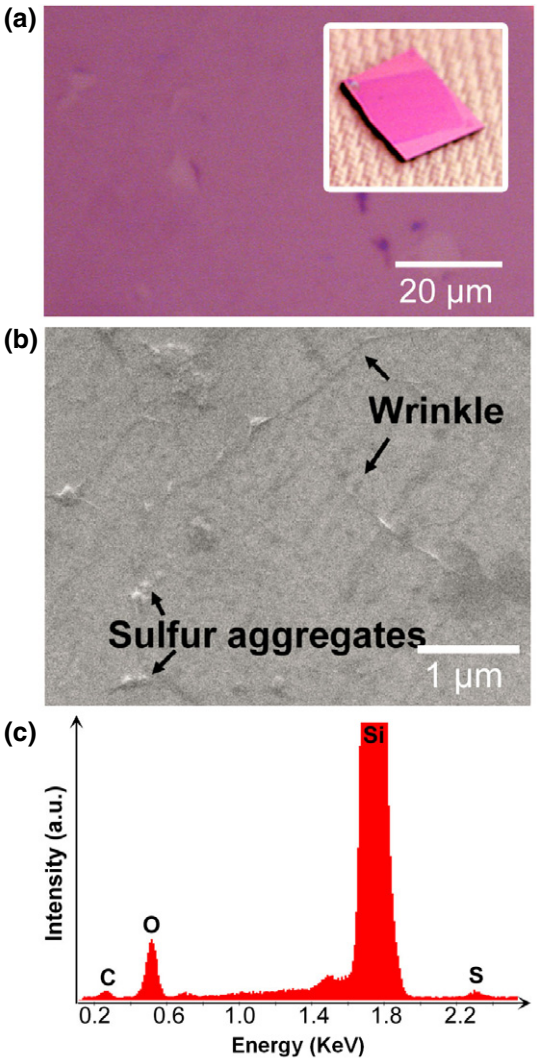

Figure 2. (a) A typical optical microscopic image of S-doped graphene on SiO_2–Si substrate. The thicknesses of the films could be distinguished by color. Inset: a photograph of S-doped graphene. (b) SEM image and (c) EDS spectrum of S-doped graphene.

zone-boundary phonons), respectively. We also observed another band, which partially merged with the G band, called the D′ band (∼1620 cm^{-1}). The band is related to the nonzero phonon density of states above the G band in graphite. After doping with S, dramatic changes were observed. (1) The intensities of the D band and D′ band for S-doped graphene were higher than those of pristine graphene. The D and D′ bands could be ascribed to substitutional doping of S atoms in the graphene lattice. (2) With respect to that of pristine graphene, the position of the 2D band for S-doped graphene had a significant upshift (∼12 cm^{-1}) and its relative intensity is generally decreased. The upshift of the 2D peak is well known to be sensitive to increasing the number of graphene layers or the doping effect. Figure 3(b) shows the excellent single Lorentzian fit in S-doped graphene, indicating that the film should be a monolayer sheet [14]. Therefore, the upshift of the 2D band could be attributed to the doping effect, and similar phenomena were observed in N- or B-doped graphene [15]. (3) The G band of S-doped graphene, which is located at 1597.2 cm^{-1}, has an upshift of (∼9 cm^{-1}) compared with that of pristine graphene. It was reported that the G band shifted slightly higher in S-doped multiwalled CNTs than in pure multiwalled CNTs, and our result had the same trend as that for S-doped CNTs [16]. When C atoms were replaced by S atoms, the C–S bond was about 25% longer than the C–C bond [4]. If only the changes in the bond length were considered, the observed G band shift for S-doped graphene was consistent with that of B-doped graphene in the fixed lattice [17]. (4) The D band shifted from 1346.3 to 1352.5 cm^{-1} after doping with S, and the upshift could be attributed to the increase in the scattering cross-section area or the defect-induced double resonant mode in the first-order spectrum causing defects, which was also observed in S-doped multiwalled CNTs [16].

The in-plane crystallite sizes (L_a) of the S-doped and pristine graphene were calculated separately by the following formula [18]:

$$L_a\ (\text{nm}) = (2.4 \times 10^{-10})\lambda^4 (I_D/I_G)^{-1}. \quad (1)$$

In the formula, λ is the Raman excitation wavelength; I_D and I_G represent the relative intensities of D and G bands. By calculation, S-doped graphene has smaller crystallite sizes (10.5 nm) than pristine graphene (27.3 nm).

The nature of binding between C and S could be confirmed by the XPS analysis. As shown in figure 4(a), the peaks at 284.5, 163.9, and 155.2 eV correspond to C 1s of sp^2 carbon, S 2p of the doping sulfur and Si 2s of the silica substrate, respectively. As shown in the inset of figure 4(a), S signal was observed in the zoom-in XPS spectrum of S-doped graphene, whereas it was not detected on the control sample (pristine graphene), indicating the successful doping of S into the graphene. The detected atomic percentage of S was very small (∼0.6 at.%), which is close to the baseline of XPS. According to the above EDS analysis, most of the S formed absorbed aggregates on the surface of the graphene. The absorbed S would be mainly removed by the vacuum during the XPS procedure. Moreover, the detected signal for S in XPS should be only related to the doping S. Our results were of the same order as that in S-doped graphite (the doping S was detected to be 0.6 at.%) [12, 13]. The inferior doping level of S was attributed to the required large formation energy between S and C atoms. According to the report of Thrower and Myer [19], the formation energy of a vacancy defect site in one unit cell is about 7 ± 0.5 eV in the graphene sheet, and formation of two vacancy defects needs more energy. Thus, the high formation energy of vacancy defects will greatly limit the S doping defects.

Figures 4(b) and (c) show the high resolution XPS spectra for C 1s and S 2p core level peaks. Careful analysis of the high resolution C 1s core level peak showed that the main peak was located at 284.5 eV, indicating that most of the C atoms remained in the conjugated honeycomb lattice, like sp^2 C in the graphite. The C peak was broadened due to the mixture of sp^2 C and C–S atoms with high binding energy (285.3 eV), which was in good agreement with that of S-doped diamond and S-containing functionality modified SWCNTs. The peak at approximately 287.8 eV was attributed to the contribution

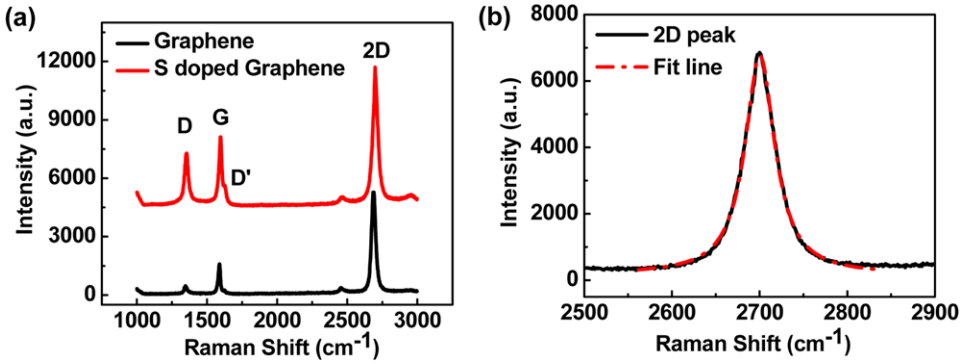

Figure 3. (a) Raman spectra of pristine graphene (black line) and S-doped graphene (red line). (b) 2D band in S-doped graphene (black line) and Lorentzian fit (red line).

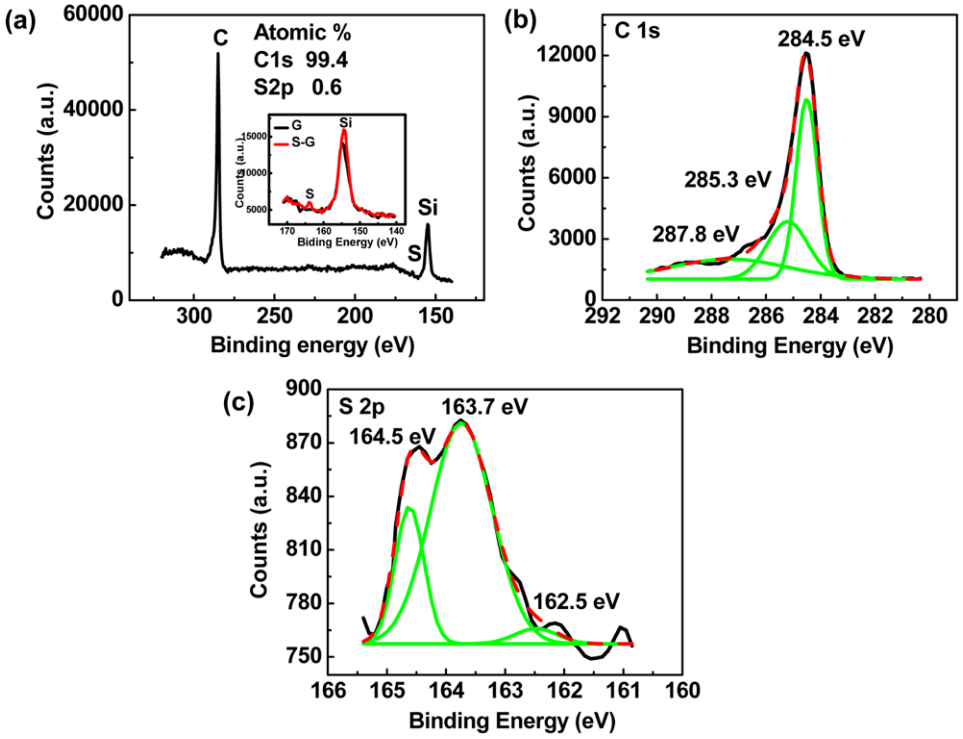

Figure 4. XPS of S-doped graphene. (a) XPS survey of S-doped graphene. The inset shows a close-up around the S peak. S-doped graphene shows a small S signal, whereas the control sample does not. (b) High resolution C 1s band, which can be divided into three Gaussian peaks at 284.5, 285.3, and 287.8 eV. (c) High resolution S 2p band, which can be deconvoluted into three Gaussian peaks at 164.5, 163.7, and 162.5 eV.

of carbonyl groups (C=O or O–C–O). During the growth of graphene or doped graphene, a small number of oxygen molecules could react with C atoms and form the C=O or O–C–O bonds. A similar phenomenon was also observed in the N-doped graphene [20]. The S 2p core level XPS spectra exhibited two primarily resolved components at 163.7 and 164.5 eV overlapping with each other. We did not observe signals with binding energy higher than 165.5 eV, which indicated that S constituents were not oxidized into sulfate or sulfite functional groups (such as SO_4^{2-} or SO_3^{2-}) [21]. Based on the previous XPS analysis for other S-doped C materials, the binding energy of the C–S band was located at about 163.7 eV, as in CS_2, C_xS compounds and S-doped graphitic C_3N_4 [22–24]. Moreover, the band at 163.7 eV was also observed in S-doped graphene, so it was reasonably derived from C–S bonds, and the band at 164.5 eV was ascribed to the neutral S, which also existed in the structure of graphene, similar to that of S-doped graphite [12].

To confirm the presence of S species in the graphene, HRTEM with elemental mapping was performed (figure 5). S-doped graphene sheet was transferred onto lacey C-coated Cu TEM grids. Most S-doped graphene sheets are single layered. Figure 5(a) shows a typical edge of single-layered graphene in a random region [25]. The selected area electron diffraction (SAED) is shown in figure 5(b). The SAED revealed a hexagonal pattern, which confirmed the threefold symmetry of the C atom arrangement. Also, some randomly distributed black regions were observed in figure 5(a) (marked

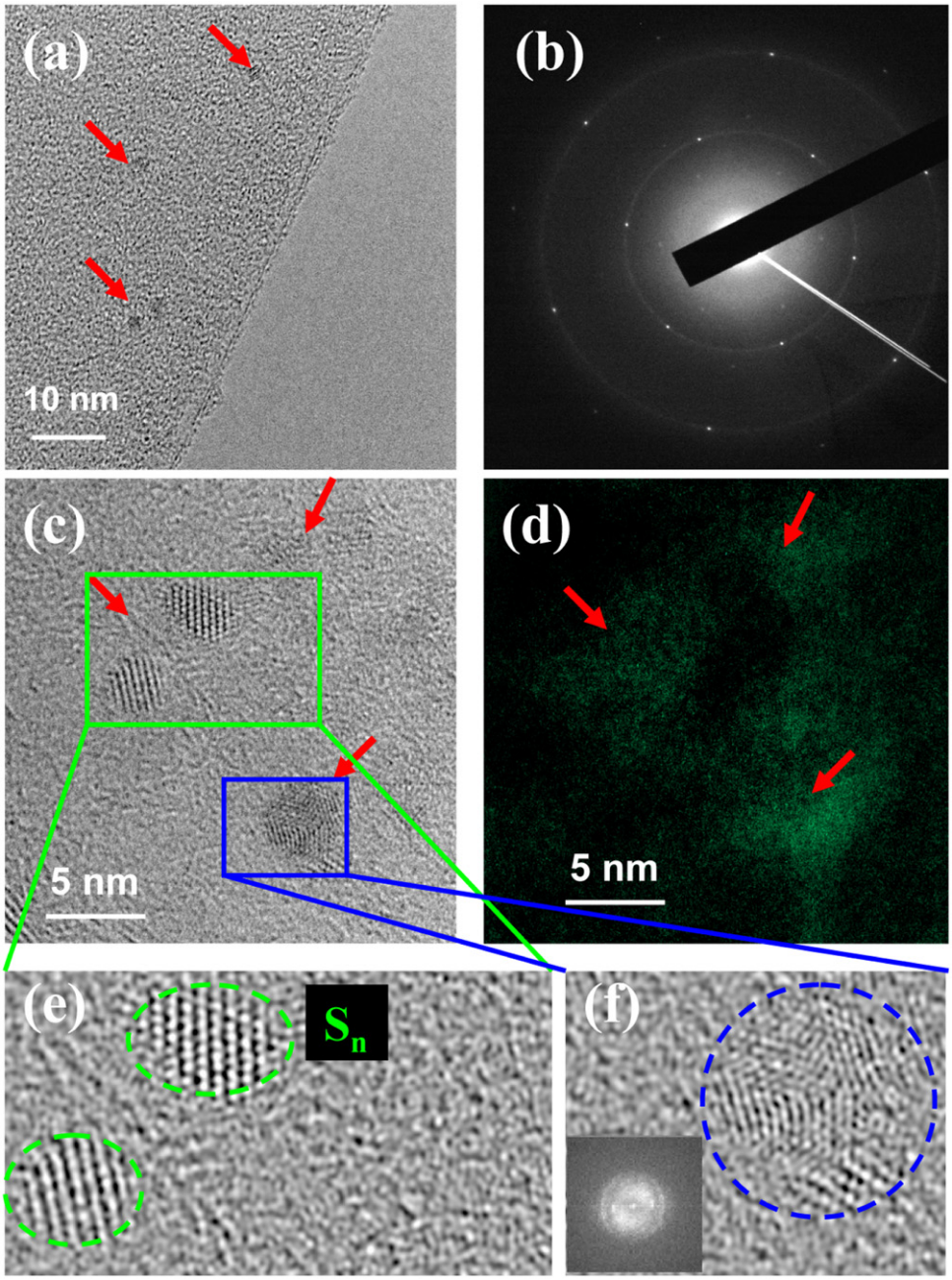

Figure 5. HRTEM and elemental analysis of S-doped graphene. (a) HRTEM image of S-doped graphene sheet; the red arrows indicate the black regions. (b) SAED image of S-doped graphene. (c) HRTEM image around the black regions. (d) Elemental mapping for (c). The distribution of S atoms is shown in green. (e), (f) The HRTEM images in green and blue square frames of (c) after FFT transformation; the inset of (f) is an FFT image of S-doped graphene. The S linear nanodomain structure is shown in the regions of the green dashed circle, and the dramatic disturbance in the graphene structure can be observed in the blue dashed circle.

by the red arrows), and the sizes of these black regions were within the range of 2–5 nm. They have been proved to be S domains by HRTEM images and elemental mapping, shown in figures 5(c) and (d). Figure 5(c) shows their lattice structure, and figure 5(d) shows their distribution on the graphene matrix in green. It seems that S atoms prefer to aggregate in the black regions. More HRTEM images around the black regions are shown in figures 5(e) and (f), and the inset of figure 5(f) is the fast Fourier transform (FFT) image. It was surprising to observe that most S atoms formed the linear nanodomains in the black region, though the number of S atoms was not regular (represented by S_n). We found that large defect regions will be formed in the graphene sheets during the growth process (figure 5(c)). These regions should easily attract more S atoms because of their lower energy. Sulfur atoms automatically arranged in the linear superlattice structure and acted as a bridge to connect the sp^2 C hexagonal lattice to form the S–graphene network. This is very interesting because rubber vulcanized by S treatment has ahe similar structure to this. During vulcanization, some of the C–H bonds are

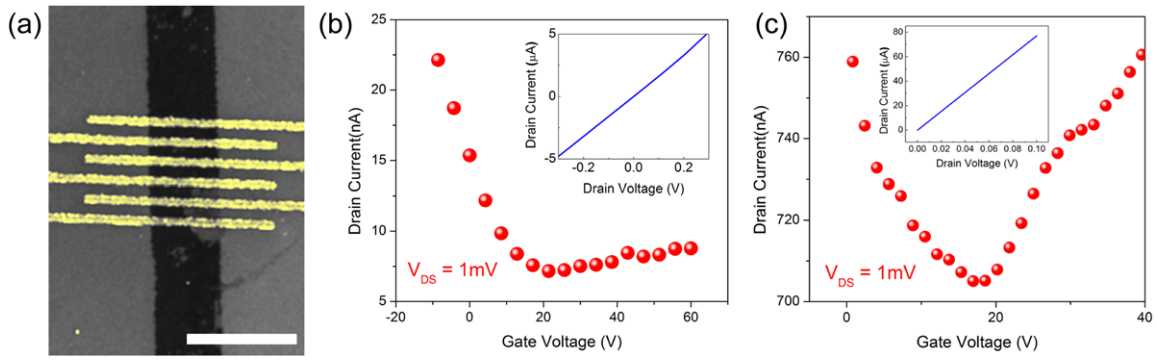

Figure 6. Electrical properties of the pristine graphene and S-doped graphene FET devices. (a) SEM image of a typical graphene FET device. Scale bar: 50 μm. (b), (c) I_{ds} versus V_g plots for both S-doped and pristine graphene FET devices. The drain voltage is fixed at 1 mV. Insets are corresponding I–V curves at zero gating voltage.

replaced by chains of S atoms, which link with a site of another polymer chain. These bridges contain between one and eight atoms. Moreover, the states of S atoms were very similar to the neutral S. The existence of S observed in HRTEM was consistent with the previous analysis of XPS.

The bottom-gated S-doped graphene FET devices (figure 6(a)) were fabricated on SiO_2–Si substrates to measure the electrical properties. In detail, the samples were transferred onto SiO_2(285 nm)–Si wafer (a), and then Ni–Au (5 nm–80 nm) electrodes were pre-patterned on it using photolithography. Graphene ribbons were fabricated by photolithography and by oxygen plasma. The FET device was measured at a probe station (Desert Cryogenic TT-probe 6 system) under vacuum (10^{-5}–10^{-6} □ Torr), connected with an Agilent 4155C semiconductor parameter analyzer. The sheet resistance of S-doped graphene is $\sim 6.28 \times 10^3$ Ω/□, lower than the reported values of pristine graphene (typically from thousands to hundreds of Ohms per square). This is possibly attributable to scattering centers in the doping defect regions. The plot of drain current versus gate voltage showed a p-type behavior for the S-doped graphene FET device (figure 6(b)), while a symmetric behavior was observed in the pristine graphene (figure 6(c)). Insets are corresponding I–V plots collected at zero gating voltage. The applied source–drain voltage is 1 mV. The mobility was estimated by $\mu = [\mathbf{d}I_{ds}/\mathbf{d}V_g] \times [L/(WC_iV_{ds})]$ [26], where L is the channel length, ∼46 μm, W is the channel width, ∼32 μm, and $C_i \sim 1.2 \times 10^{-8}$ F cm^{-2} is the capacitance per unit area between the channel and the back-gate. The calculated mobility range was ∼90 cm^2 V^{-1} s^{-1}, less than that of pristine graphene (100–2000 cm^2 V^{-1} s^{-1}, figure 6(h)) [27]. The S-doped graphene has larger on/off ratio than the pristine graphene. This may be caused by the absorbed S atoms and relative doping introduced defects [28, 29]. However, it is still unclear how the absorbed S or S atoms in the nanodomains dominated the electronic transport in the graphene, and further investigations and theoretical calculation are needed.

4. Conclusion

In conclusion, we have demonstrated a simple methodology for synthesizing larger area and mostly single layer S-doped graphene sheets. The novel liquid precursor synthesis route could prove highly advantageous in doping graphene. We proposed that S atoms were tending to form linear nanodomains in graphene's lattice. Sulfur atom doping modified the structure of graphene, and the as-prepared S-doped graphene exhibited higher resistance and p-type semiconductor behavior, which was quite different from that of the pristine graphene. This work is anticipated to open a new possibility in the investigation of S-doped graphene and could have potential application in addressing various electronic issues.

Acknowledgments

This work was financially supported by the Fundamental Research Funds for the Central Universities (lzujbky-2011-52) and the Key Laboratory of Materials for High-Power Laser, Shanghai Institute of Optics and Fine Mechanics. PMA and ZL acknowledge funding support from the Office of Naval Research through the MURI program on graphene.

References

[1] Régis Y N G, Konstantinos S and Petra R 2010 *J. Phys. D: Appl. Phys.* **43** 374015
[2] Martin T B, Miwa R H, Antônio J R D S and Fazzio A 2007 *Phys. Rev. Lett.* **98** 196803
[3] Kurmaev E Z, Galakhov A V, Moewes A, Moehlecke S and Kopelevich Y 2002 *Phys. Rev.* B **66** 193402
[4] Denis P A 2010 *Chem. Phys. Lett.* **492** 251
[5] Denis P A, Faccio R and Mombru A W 2009 *ChemPhysChem* **10** 715
[6] Ao Z M, Yang J, Li S and Jiang Q 2008 *Chem. Phys. Lett.* **461** 276
[7] Dai J Y, Yuan J M and Giannozzi P 2009 *Appl. Phys. Lett.* **95** 232105
[8] Hasegawa M, Takeuchi D, Yamanaka S, Ogura M, Watanabe H, Kobayashi N, Okushi H and Kajimura K 1999 *Japan. J. Appl. Phys.* **38** L1519
[9] Sakaguchi I, Gamo M N, Kikuchi Y, Yasu E and Haned H 1999 *Phys. Rev.* B **60** R2139
[10] Glenis S, Cooke S, Chen X and Labes M M 1996 *Chem. Mater.* **8** 123
[11] Silva R R, Torres J H S and Kopelevich Y 2001 *Phys. Rev. Lett.* **87** 147001

[12] Glenis S, Nelson A J and Labes M M 1999 *J. Appl. Phys.* **86** 4464
[13] Nakamura T, Ohana T, Ishihara M, Hasegawa M and Koga Y 2007 *Diamond Relat. Mater.* **6** 1091
[14] Ferrari A C *et al* 2006 *Phys. Rev. Lett.* **97** 187401
[15] Robison J A 2009 *Nano Lett.* **9** 964
[16] Curran S A, Cech J, Zhang D, Dewald J L, Avadhanula A, Kandadai M and Roth S 2006 *J. Mater. Res.* **21** 1012
[17] Terrones M, Jorio A, Endo M, Rao A M, Kim Y A, Hayashi T, Terrones H, Charlier J-C, Dresselhaus G and Dresselhaus M S 2004 *Mater. Today* **7** 30
[18] Cançado L G, Takai K, Enoki T, Endo M, Kim Y A, Mizusaki H, Jorio A, Coelho L N, Magalhães-Paniago R and Pimenta M A 2006 *Appl. Phys. Lett.* **88** 163106
[19] Thrower P A and Mayer R M 1978 *Phys. Status Solidi* a **47** 11
[20] Wang Y, Shao Y Y, Matson D W, Li J H and Lin Y H 2010 *ACS Nano* **4** 1790
[21] Gupta S, Weiner B R and Morell G 2003 *J. Mater. Res.* **18** 363
[22] Shin H J *et al* 2009 *Adv. Funct. Mater.* **19** 1987
[23] Liu G, Niu M, Sun C, Smith S C, Chen Z, Lu G Q and Cheng H M 2010 *J. Am. Chem. Soc.* **132** 11642
[24] Chanc C H 1981 *Carbon* **19** 175
[25] Srivastava A, Galande C, Ci L J, Song L, Rai C, Jariwala D, Kelly K F and Ajayan P M 2010 *Chem. Mater.* **22** 3457
[26] Wei D H, Liu Y Q, Wang Y, Zhang H L, Huang L P and Yu G 2009 *Nano Lett.* **9** 1752
[27] Reina A, Jia X, Ho J, Nezich D, Son H, Bulovic V, Dresselhaus M S and Kong J 2008 *Nano Lett.* **9** 30
[28] Martins T B, Miwa R H, Silva A J R and Fazzio A 2007 *Phys. Rev. Lett.* **98** 196803
[29] Gomez-Navarro C, Weitz R T, Bittner A M, Scolari M, Mew A, Burghard M and Kern K 2007 *Nano Lett.* **7** 3499